

The Thin Film Flow of Walter's B Fluid over the Surface of a Stretching Cylinder with Heat and Mass Transfer Analysis

Khan W^{1*} and Gul T²

¹Département of Mathematics, Islamia College Peshawar, Kyber Pakhtunkhwa, Pakistan

²Department of Mathematics, City University of Science and Information Technology (CUSIT), Pakistan

Abstract

The main objective of this work is to study the performance of the boundary layer flow considering non-Newtonian Walter's B fluid over the surface of an unstable cylinder to protect the surface of the cylinder from external heating and cooling. The Soret and Dufour properties with heat and mass transmission have been encountered in the flow field. Using the appropriate similarity transformations the leading PDE's for the flow field have been altered into high ordered non-linear coupled ODE's. Series solutions of the subsequent problem are computed by using controlling procedure homotopy analysis method. The properties of the included physical parameters in the problem, like Reynolds number, Walter's B fluid parameter, Prandtl number, Schmidt numbers, Dufour and Soret numbers have been illustrated. The behavior of Skin friction, Sherwood number and local Nusselt number have been described numerically for the dynamic constraints of the problem and the comparison of these physical parameters have been displayed with the experimental consequences in the existent literature. The optimal convergence of the applied method has been patterned by plotting h-curves. Finally, the results, obtained from HAM, have been justified through numerical (ND-Solve) method and tabulated comparison.

Keywords: Heat and mass transfer flow of the Walter's B fluids; Liquid film; Unstable stretching cylinder; Skin friction; Local nusselt and sherwood numbers; HAM and numerical method

Introduction

Thin film flow is one of important natural phenomena. Its enormous usages and application in the expanse of industries, engineering and technology in a last few years clarify its importance in nature. The analysis of thin film flow of practical applications is a challenging interplay between fluid mechanics and fluid dynamic. Wire and fibre coating is one of its important applications. Extrusion of polymer and metal, processing of food stuff, continuous casting, plastic sheets drawing, and fluidization of reactor, exchanges, and chemical processing equipment are some of its common applications. Keeping in view such a countless applications researcher did a lot of work on it. Wang [1] was the main researcher to investigate liquid film on a time dependent stretching sheet. The similar work was further improved by Ushah and Sridharan [2]. The heat transmission effect on liquid film analysis on horizontal sheet was studied by Liu and Andersson [3]. In their work they used numerical methods to obtain the solution and also discuss the confined flow parameters. Aziz et al. [4] perceived the consequence of inner heat production of a thin liquid film flow on a time dependent stretched sheet. Recently Tawade et al. [5] examined thin liquid flow over an un-steady stretched sheet with thermal radiation, in the presence of magnetic field using RK-Fehlberg and Newton-Raphson schemes for solution of non-linear equations.

Thin fluid film flow of Non-Newtonian liquid increases in many life geographies which is used mostly in cylindrical shapes. Several researcher [6-9] investigated Power law fluid by using different cases in unsteady stretching surface. Meghahe [10] and Abolbashari et al. [11] scrutinized thin film flow of Caisson fluid flows and heat transmission in the existence of inconsistency heat flux and viscid dissipation with slip velocity. Recently Qasim et al. [12] deliberates the Nano-fluid thin film on a time dependent stretched surface taking the Buongiorno's model.

Walter's B fluid is one of the important subclasses of non-

Newtonian fluids. Several researchers investigated Walter's B fluid with effect of heat and MHD. Very less study is available on it in the form of thin films flow in cylinder. Hussain and Ullah [13] examined boundary layer flow using Walter's B fluid on a stretched cylinder with temperature reliant viscosity. Manjunatha et al. [14] studied thermal dusty fluid flow over a permeable stretched cylinder in the occurrence of non-uniform source or sink. Hayat et al. [15] investigated axisymmetric third order liquid flow on a stretching cylinder within the effect of MHD. Qasim et al. [16] considered the MHD Boundary Layer having Slip condition Flow under Heat Transition of the Ferrofluid on a Stretching Cylinder with a suggested Heat Flux. Sheikholeslami [17] studied the consequence of constant value of suction of Nano-fluid flows and heat transition over a stretched pipe. Manjunatha et al. [18] studied the radiation influence and heat transmission of MHD Dusty Fluid flow over a Stretched Cylinder Surrounded in a Porous Medium in the occurrence of Heat Sources. Abdulhameed et al. [19] considered the oscillating and heat transmission and association of different pressure waveforms in a circular cylinder. Mahdy [20] examined heat transmission of a Casson fluid flow over a stretched cylinder while considering dufour and soret effects. Abdul Hakeem et al. [21] observed the influence of heat radioactivity of Walter's B fluid on a stretched surface with non-uniform heat source/sink and flexible deformation. Pandey et al. [22] deliberate the Features of Walter's B Visco-Elastic Nano-fluid Layer and Heat transition.

In the field of engineering most of mathematical problems are

***Corresponding author:** Khan W, Département of Mathematics, Islamia College Peshawar, Kyber Pakhtunkhwa 25000, Pakistan, Tel: 92-3028397271; E-mail: wariaskhan758@yahoo.com

Received July 23, 2017; **Accepted** July 31, 2018; **Published** August 08, 2018

Citation: Khan W, Gul T (2018) The Thin Film Flow of Walter's B Fluid over the Surface of a Stretching Cylinder with Heat and Mass Transfer Analysis. J Appl Computat Math 7: 411. doi: [10.4172/2168-9679.1000411](https://doi.org/10.4172/2168-9679.1000411)

Copyright: © 2018 Khan W, et al. This is an open-access article distributed under the terms of the Creative Commons Attribution License, which permits unrestricted use, distribution, and reproduction in any medium, provided the original author and source are credited.

complex in nature and the exact solution is almost very difficult or even not possible. So Numerical and Analytical methods are used to find the approximate solution. In these methods Homotopy Analysis Method is one of the important and popular techniques for the solution of such type of problems. It is an auxiliary method and its foremost advantage is to apply on the differential equations which are nonlinear without discretization and linearization. Liao [23-30] investigated this technique for the answer of non-linear equations and successfully proved that this method is rapidly convergent to the approximated solutions. Apart from this, this method provides series solutions in the form of single variable functions. Finding solution with this method is important because it involves all the physical parameters of the problem and we can easily discuss its behaviour. The authors [31-34] used this procedure to answer highly non-linear and coupled equations due to its fast convergence.

As it is already mentioned that most of the published work related to thin films are available about viscous fluids in Cartesian systems, where very less literature is available on the non-Newtonian fluids in Cylindrical system. The advancement of research in the field of thin films and its application in industry and technology is the need of the existing era. Therefore, the determination of existing research is based on the study of non-Newtonian thin film flow in cylindrical system. So, for this aim Walter's B fluid flow is considered [35]. HAM is used for the solution modelled equations which are nonlinear and coupled. The effect of modelled parameters has been studied graphically [36].

Problem Formulation

Consider the steady axi-symmetric and incompressible flow of Walter's B fluid in a stretched cylinder having radius a alongside axial direction, where z is alongside cylinder and r is along to radial direction. The temperature at the cylinder surface is represented by T_b and the concentration is symbolized by C_b respectively. The stretching velocity of the cylinder is $W_w = 2cz$, in which $c > 0$ represented the stretched constant, the size of the cylinder condenses but the outside radius of the pipe are taken fixed. $T = T_b - T_r \left(\frac{cz^2}{v_{wf}} \right) \Theta(\zeta)$, $C = C_b - C_r \left(\frac{cz^2}{v_{wf}} \right) \Phi(\zeta)$ is

the temperature and concentration fields, in which T_b, C_b is the initial temperature and concentration and T_r, C_r is the reference temperature and concentration respectively. Viscous dissipation and the body forces are neglected in the flow field. Also, supposition is made that the base fluid and the nanometer size particle exist in thermal equilibrium, dominate the deficiency of slip.

Considering these suppositions in cylindrical coordinates (γ, z) , the mass of conservation equation, the conservation of momentum equation, energy and concentration equations can be identified as:

$$\frac{\partial(ru)}{\partial r} + \frac{\partial(rw)}{\partial z} = 0, \tag{1}$$

$$\begin{aligned} \rho \left[u \frac{\partial w}{\partial r} + w \frac{\partial w}{\partial z} \right] &= \frac{1}{r} \left\{ \eta_0 \left(\frac{\partial u}{\partial z} + \frac{\partial w}{\partial r} \right) - k_0 u \left(\frac{\partial^2 u}{\partial r \partial z} + \frac{\partial^2 w}{\partial r^2} \right) - k_0 w \left(\frac{\partial^2 u}{\partial z^2} + \frac{\partial^2 w}{\partial z \partial r} \right) \right\} \\ &+ \frac{\partial}{\partial r} \left\{ \eta_0 \left(\frac{\partial u}{\partial z} + \frac{\partial w}{\partial r} \right) - k_0 u \left(\frac{\partial^2 u}{\partial r \partial z} + \frac{\partial^2 w}{\partial r^2} \right) - k_0 w \left(\frac{\partial^2 u}{\partial z^2} + \frac{\partial^2 w}{\partial z \partial r} \right) \right\} \tag{2} \\ &+ \frac{\partial}{\partial z} \left\{ \eta_0 \left(\frac{\partial u}{\partial z} + \frac{\partial w}{\partial r} \right) - 2k_0 u \frac{\partial^2 w}{\partial r \partial z} - 2k_0 w \frac{\partial^2 w}{\partial z^2} \right\}, \end{aligned}$$

$$\begin{aligned} \rho \left[u \frac{\partial u}{\partial r} + w \frac{\partial u}{\partial z} \right] &= -\frac{\partial p}{\partial r} + \frac{2\eta_0}{r} \frac{\partial u}{\partial r} - \frac{2k_0}{r} u \frac{\partial^2 u}{\partial r^2} - \frac{2k_0}{r} w \frac{\partial^2 u}{\partial z \partial r} \\ &+ \frac{\partial}{\partial r} \left\{ 2\eta_0 \frac{\partial u}{\partial r} - 2k_0 u \frac{\partial^2 u}{\partial z \partial r} - 2k_0 w \frac{\partial^2 u}{\partial z \partial r} \right\} \tag{3} \\ &- \frac{\partial}{\partial z} \left\{ \eta_0 \left(\frac{\partial u}{\partial z} + \frac{\partial w}{\partial r} \right) - k_0 u \left(\frac{\partial^2 u}{\partial r \partial z} + \frac{\partial^2 w}{\partial z \partial r} \right) - k_0 w \left(\frac{\partial^2 u}{\partial z^2} + \frac{\partial^2 w}{\partial z \partial r} \right) \right\} \\ &- \frac{2\eta_0}{r^2} u - \frac{2k_0}{r^3} u^2 - \frac{2k_0}{r^2} \frac{\partial u}{\partial z}, \end{aligned}$$

$$w \frac{\partial T}{\partial z} + u \frac{\partial T}{\partial r} = \alpha \left(\frac{\partial^2 T}{\partial r^2} + \frac{1}{r} \frac{\partial T}{\partial r} \right) + \frac{D_k}{c_p c_s} \left(\frac{\partial^2 C}{\partial r^2} + \frac{1}{r} \frac{\partial C}{\partial r} \right), \tag{4}$$

$$w \frac{\partial C}{\partial z} + u \frac{\partial C}{\partial r} = D \left(\frac{\partial^2 C}{\partial r^2} + \frac{1}{r} \frac{\partial C}{\partial r} \right) + \frac{D_k}{T_m} \left(\frac{\partial^2 T}{\partial r^2} + \frac{1}{r} \frac{\partial T}{\partial r} \right). \tag{5}$$

The applicable Boundary Constrains for the flow pattern are taken as:

$$\begin{aligned} u = U_w, w = W_w, T = T_w, C = C_w \text{ at } r = a \\ \frac{\partial w}{\partial r} = \frac{\partial T}{\partial r} = \frac{\partial C}{\partial r} = \frac{\partial \sigma}{\partial r} = 0, u = \frac{d\sigma}{dz} \text{ at } r = b \end{aligned} \tag{6}$$

Taking $u(\gamma, z)$ and $w(\gamma, z)$ are the velocities components, ρ indicates the density of the fluid, k_0 indicates the thermal conductivity, p is the pressure, α represents the thermal diffusivity, T denotes the local temperature, σ indicates thickness of the fluid film, C_p is mentioned for specific heat, C_s is used for concentration susceptibility, D indicates the mass diffusivity, C symbolizes concentration field, where is T_m represents the mean temperature of the fluid.

Familiarising the succeeding similarity transformations:

$$\begin{aligned} \zeta = \left(\frac{r}{a} \right)^2, w = 2cf'(\zeta)z, u = -\frac{ca}{\sqrt{\zeta}} f(\zeta), \\ \Theta(\zeta) = \frac{T - T_b}{T_a - T_b}, \Phi(\zeta) = \frac{C - C_b}{C_a - C_b}. \end{aligned} \tag{7}$$

The prime identifies the derivative w.r.t the similarity variable ζ , $c > 0$ indicates stretching constraint, a specifies exterior radius of cylinder where the exterior radius is represented by b . $f(\zeta), \Theta(\zeta), \Phi(\zeta)$ Indicate the non-dimensional velocity profile, temperature gradient and concentration field.

Using the similarity transformation i.e., eqn. (7) in eqns. (1-6), justifies the mass of conservation equation automatically and the left over equations are transformed to non-linear ordinary differential scheme as:

$$2\zeta \left(\frac{d^3 f}{d\zeta^3} + \frac{d^2 f}{d\zeta^2} \right) + \text{Re} \zeta^2 \left[f \frac{d^2 f}{d\zeta^2} - \left(\frac{df}{d\zeta} \right)^2 \right] + 2A \zeta \frac{d^2 f}{d\zeta^2} \frac{d^3 f}{d\zeta^3} + 2A \left(\frac{d^2 f}{d\zeta^2} \right)^2 + \tag{8}$$

$$\begin{aligned} 4A \zeta f \frac{d^3 f}{d\zeta^3} + 4A \zeta^2 f \frac{d^4 f}{d\zeta^4} - A \zeta f \frac{d^2 f}{d\zeta^2} - 2A \zeta \frac{df}{d\zeta} \frac{d^2 f}{d\zeta^2} = 0 \\ \zeta \frac{d^2 \Theta}{d\zeta^2} + \frac{d\Theta}{d\zeta} + \text{Re Pr} \left[f \frac{d\Theta}{d\zeta} - 2 \frac{df}{d\zeta} \Theta \right] + D_u \text{Pr} \left[\frac{d\Phi}{d\zeta} + \zeta \frac{d^2 \Phi}{d\zeta^2} \right] = 0, \tag{9} \end{aligned}$$

$$\zeta \frac{d^2 \Phi}{d\zeta^2} + \frac{d\Phi}{d\zeta} + \text{Re} S_c \left[f \frac{d\Phi}{d\zeta} - 2 \frac{df}{d\zeta} \Phi \right] + S_c S_r \left[\frac{d\Theta}{d\zeta} + \zeta \frac{d^2 \Theta}{d\zeta^2} \right] = 0. \tag{10}$$

The non-dimensional boundary condition of the problem are:

$$\begin{aligned} f(1) = 0, f'(1) = 1, f''(\beta) = 0, \\ \Theta(1) = 1, \Theta'(\beta) = 0, \Phi(1) = 1, \Phi'(\beta) = 0. \end{aligned} \tag{11}$$

The physical non-dimensional parameter after simplification:

Where, $Re = \frac{ca^2}{2\nu}$ represents the Reynolds quantities, $A = \frac{k_0 c}{\eta_0}$ is Walter's B fluid constraint, $Pr = \frac{\nu}{\alpha}$ designates the Prandtl number, $D_u = \frac{D_k(C_a - C_b)}{T_m \nu(T_a - T_b)}$ represents the Dufour number, $S_c = \frac{\nu}{D}$ denotes the Schmidt number and $\frac{D_k(C_a - C_b)}{T_m(T_a - T_b)}$ is used for the Soret number.

The Skin friction value, local Nusselt number and Sherwood number can be expressed for the given flow problem as:

$$C_f = \frac{2\nu}{W_w} \left(\frac{\partial w}{\partial r} \right)_{r=a}, Nu = -\frac{ak}{(T_w - T_b)} \left(\frac{\partial T}{\partial r} \right)_{r=a}, Sh = -\frac{a}{2(C_w - C_b)} \left(\frac{\partial C}{\partial r} \right)_{r=a} \quad (12)$$

The non-dimensional forms for the above mentioned physical properties are:

$$\frac{Z Re}{a} C_f = f''(1), Nu = -2k\Theta'(1), Sh = -\Phi'(1) \quad (13)$$

Where $Re = \frac{ca^2}{2\nu}$ is the local Reynolds number.

Solution by HAM

The boundary condition in eqn. (11), are answered approximately by Homotopy Analysis Method (HAM). The solutions enclose the auxiliary parameters \hbar which is used to stabilise and adjust the convergence of solutions eqns. (8-10).

The initial solutions are chosen as follow:

$$f_0(\zeta) = \zeta - 1, \Theta_0(\zeta) = 1 \text{ and } \Phi_0(\zeta) = 1. \quad (14)$$

The linear operator for the problem are denoted by $\mathcal{L}_f, \mathcal{L}_\Theta, \mathcal{L}_\Phi$

$$\mathcal{L}_f = \frac{d^3 f}{d\zeta^3}, \mathcal{L}_\Theta = \frac{d^2 \Theta}{d\zeta^2}, \mathcal{L}_\Phi = \frac{d^2 \Phi}{d\zeta^2} \quad (15)$$

Which has given the following general solution:

$$\mathcal{L}_f(k_1 + k_2\zeta + k_3\zeta^2) = 0, \mathcal{L}_\Theta(k_4 + k_5\zeta) = 0 \text{ and } \mathcal{L}_\Phi(k_6 + k_7\zeta) = 0. \quad (16)$$

Where $k_j(j=1 \rightarrow 7)$ are constant:

The subsequent non-linear operators N_f, N_Θ, N_Φ for the problem are selected in the below given form:

$$N_f[f(\zeta; \rho)] = 2\zeta \left(\frac{d^3 f}{d\zeta^3} + \frac{d^2 f}{d\zeta^2} \right) + Re \zeta^2 \left[f \frac{d^2 f}{d\zeta^2} - \left(\frac{df}{d\zeta} \right)^2 \right] + 2A \zeta \frac{d^2 f}{d\zeta^2} \frac{d^3 f}{d\zeta^3} + 2A \left(\frac{d^2 f}{d\zeta^2} \right)^2 + 4A \zeta f \frac{d^3 f}{d\zeta^3} + 4A \zeta^2 f \frac{d^4 f}{d\zeta^4} - A \zeta f \frac{d^2 f}{d\zeta^2} - 2A \zeta \frac{df}{d\zeta} \frac{d^2 f}{d\zeta^2}, \quad (17)$$

$$N_\Theta[f(\zeta; \rho), \Theta(\zeta; \rho), \Phi(\zeta; \rho)] = \zeta \frac{d^2 \Theta}{d\zeta^2} + \frac{d\Theta}{d\zeta} + Re Pr \left[f \frac{d\Theta}{d\zeta} - 2 \frac{df}{d\zeta} \Theta \right] + D_u Pr \left[\frac{d\Phi}{d\zeta} + \frac{d^2 \Phi}{d\zeta^2} \right], \quad (18)$$

$$N_\Phi[f(\zeta; \rho), \Theta(\zeta; \rho), \Phi(\zeta; \rho)] = \zeta \frac{d^2 \Phi}{d\zeta^2} + \frac{d\Phi}{d\zeta} + Re S_c \left[f \frac{d\Phi}{d\zeta} - 2 \frac{df}{d\zeta} \Phi \right] + S_c S_r \left[\frac{d\Theta}{d\zeta} + \frac{d^2 \Theta}{d\zeta^2} \right]. \quad (19)$$

The basic idea for HAM solution is defined in eqns. (23-30), where is the Zeroth-order system for eqn. (8-10) as:

$$(1 - \rho) \mathcal{L}_f [f(\zeta; \rho) - f_0(\zeta)] = \rho \lambda_f N_f [f(\zeta; \rho)], \quad (20)$$

$$(1 - \rho) \mathcal{L}_\Theta [\Theta(\zeta; \rho) - \Theta_0(\zeta)] = \rho \lambda_\Theta N_\Theta [f(\zeta; \rho), \Theta(\zeta; \rho), \Phi(\zeta; \rho)], \quad (21)$$

$$((1 - \rho) \mathcal{L}_\Phi [\Phi(\zeta; \rho) - \Phi_0(\zeta)] = \rho \lambda_\Phi N_\Phi [f(\zeta; \rho), \Theta(\zeta; \rho), \Phi(\zeta; \rho)]. \quad (22)$$

The equivalent boundary condition for the system of equation are:

$$f(\zeta; \rho)|_{\zeta=1} = 0, \left. \frac{df(\zeta; \rho)}{d\zeta} \right|_{\zeta=1} = 1, \left. \frac{d^2 f(\zeta; \rho)}{d\zeta^2} \right|_{\zeta=\beta} = 0, \quad (23)$$

$$\Theta(\zeta; \rho)|_{\zeta=0} = 1, \left. \frac{d\Theta(\zeta; \rho)}{d\eta} \right|_{\zeta=\beta} = 0, \Phi(\zeta; \rho)|_{\zeta=1} = 1, \left. \frac{d\Phi(\zeta; \rho)}{d\zeta} \right|_{\zeta=\beta} = 0$$

Where $\rho \in [0, 1]$ is the embedding constraint, $\lambda_f, \lambda_\Theta, \lambda_\Phi$ are the axillary constraints use for the convergence of the results. For $\rho=0$ and $\rho=1$ we get:

$$f(\zeta; 1) = f(\zeta), \Theta(\zeta; 1) = \Theta(\zeta), \Phi(\zeta; 1) = \Phi(\zeta). \quad (24)$$

Expand the non-dimensional velocity, temperature and concentration fields $f(\zeta; \rho), \Theta(\zeta; \rho), \Phi(\zeta; \rho)$ by Taylor's series when.

$$f(\zeta; \rho) = f_0(\zeta) + \sum_{\sigma=1}^{\infty} f_\sigma(\zeta) \rho^\sigma, \quad (25)$$

$$\Theta(\zeta; \rho) = \Theta_0(\zeta) + \sum_{\sigma=1}^{\infty} \Theta_\sigma(\zeta) \rho^\sigma,$$

$$\Phi(\zeta; \rho) = \Phi_0(\zeta) + \sum_{\sigma=1}^{\infty} \Phi_\sigma(\zeta) \rho^\sigma.$$

Where

$$f_\sigma(\zeta) = \frac{1}{\sigma!} \left. \frac{d^\sigma f(\zeta; \rho)}{d\zeta^\sigma} \right|_{\rho=0}, \Theta_\sigma(\zeta) = \frac{1}{\sigma!} \left. \frac{d^\sigma \Theta(\zeta; \rho)}{d\zeta^\sigma} \right|_{\rho=0}, \Phi_\sigma(\zeta) = \frac{1}{\sigma!} \left. \frac{d^\sigma \Phi(\zeta; \rho)}{d\zeta^\sigma} \right|_{\rho=0}. \quad (26)$$

The axillary parameter $\lambda_f, \lambda_\Theta, \lambda_\Phi$ are designated in a fashion that the series in eqn. (25) converges at $\rho = 1$ injecting $\rho = 1$ in eqn. (25), we achieve:

$$f(\zeta; \rho) = f_0(\zeta) + \sum_{\sigma=1}^{\infty} f_\sigma(\zeta), \quad (27)$$

$$\Theta(\zeta; \rho) = \Theta_0(\zeta) + \sum_{\sigma=1}^{\infty} \Theta_\sigma(\zeta),$$

$$\Phi(\zeta; \rho) = \Phi_0(\zeta) + \sum_{\sigma=1}^{\infty} \Phi_\sigma(\zeta) \rho^\sigma.$$

The σ th - order system for eqn. (8-10) are the following:

$$\mathcal{L}_f [f_\sigma(\zeta) - N_\sigma f_{\sigma-1}(\zeta)] = \lambda_f \mathfrak{R}_\sigma^f(\zeta), \quad (28)$$

$$\mathcal{L}_\Theta [\Theta_\sigma(\zeta) - N_\sigma \Theta_{\sigma-1}(\zeta)] = \lambda_\Theta \mathfrak{R}_\sigma^\Theta(\zeta),$$

$$\mathcal{L}_\Phi [\Phi_\sigma(\zeta) - N_\sigma \Phi_{\sigma-1}(\zeta)] = \lambda_\Phi \mathfrak{R}_\sigma^\Phi(\zeta).$$

The consistent boundary conditions are:

$$f_\sigma(1; \rho) = \frac{df_\sigma(1; \rho)}{d\zeta} = \frac{d^2 f_\sigma(\beta; \rho)}{d\zeta^2} = 0, \quad (29)$$

$$\Theta_\sigma(1; \rho) = \frac{d\Theta_\sigma(\beta; \rho)}{d\zeta} = \Phi_\sigma(1; \rho) = \frac{d\Phi_\sigma(\beta; \rho)}{d\zeta} = 0.$$

Here

$$\mathfrak{R}_\sigma^f(\zeta) = 2\zeta \left(\frac{d^3 f_{\sigma-1}}{d\zeta^3} + \frac{d^2 f_{\sigma-1}}{d\zeta^2} \right) + Re \zeta^2 \left(\sum_{k=1}^{\sigma-1} f_{\sigma-1-k} \frac{d^2 f_k}{d\zeta^2} - \sum_{k=1}^{\sigma-1} \frac{df_{\sigma-1-k}}{d\zeta} \frac{d^2 f_k}{d\zeta^2} \right) + 2A \sum_{k=1}^{\sigma-1} \frac{d^2 f_{\sigma-1-k}}{d\zeta^2} \frac{d^2 f_k}{d\zeta^2} + 4A \zeta \sum_{k=1}^{\sigma-1} f_{\sigma-1-k} \frac{d^3 f_k}{d\zeta^3} + 4A \zeta^2 \sum_{k=1}^{\sigma-1} f_{\sigma-1-k} \frac{d^4 f_k}{d\zeta^4} - A \zeta \sum_{k=1}^{\sigma-1} f_{\sigma-1-k} \frac{d^2 f_k}{d\zeta^2} - 2A \zeta \sum_{k=1}^{\sigma-1} \frac{df_{\sigma-1-k}}{d\zeta} \frac{d^2 f_k}{d\zeta^2}, \quad (30)$$

$$\mathfrak{H}_m^\Theta(\zeta) = \zeta \frac{d^2\Theta_{\sigma-1}}{d\zeta^2} + \frac{d\Theta_{\sigma-1}}{d\zeta} + \text{Re Pr} \left(\sum_{\kappa=1}^{\sigma-1} f_{\sigma-1-\kappa} \frac{d\Theta_\kappa}{d\zeta} - 2 \sum_{\kappa=1}^{\sigma-1} \frac{df_{\sigma-1-\kappa}}{d\zeta} \Theta_\kappa \right) + D_u \text{Pr} \left(\frac{d\Phi_{\sigma-1}}{d\zeta} + \zeta \frac{d^2\Phi_{\sigma-1}}{d\zeta^2} \right), \quad (31)$$

$$\mathfrak{H}_m^\Phi(\zeta) = \zeta \frac{d^2\Phi_{\sigma-1}}{d\zeta^2} + \frac{d\Phi_{\sigma-1}}{d\zeta} + \text{Re S}_c \left(\sum_{\kappa=1}^{\sigma-1} f_{\sigma-1-\kappa} \frac{d\Phi_\kappa}{d\zeta} - 2 \sum_{\kappa=1}^{\sigma-1} \frac{df_{\sigma-1-\kappa}}{d\zeta} \Phi_\kappa \right) + S_c S_r \left(\frac{d\Theta_{\sigma-1}}{d\zeta} + \zeta \frac{d^2\Theta_{\sigma-1}}{d\zeta^2} \right), \quad (32)$$

Where

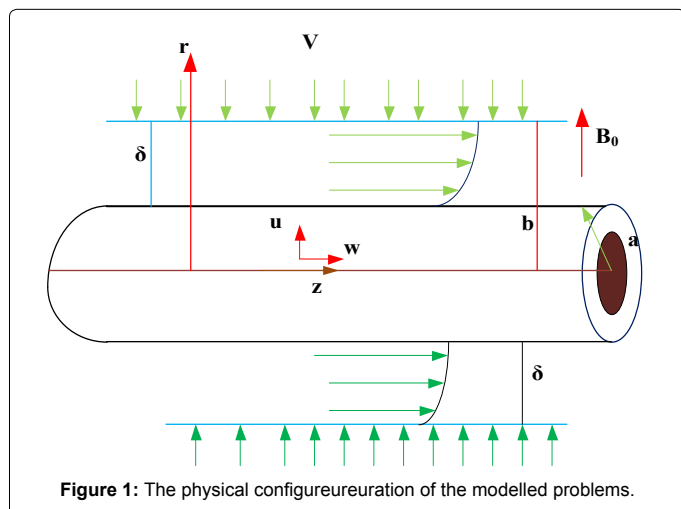
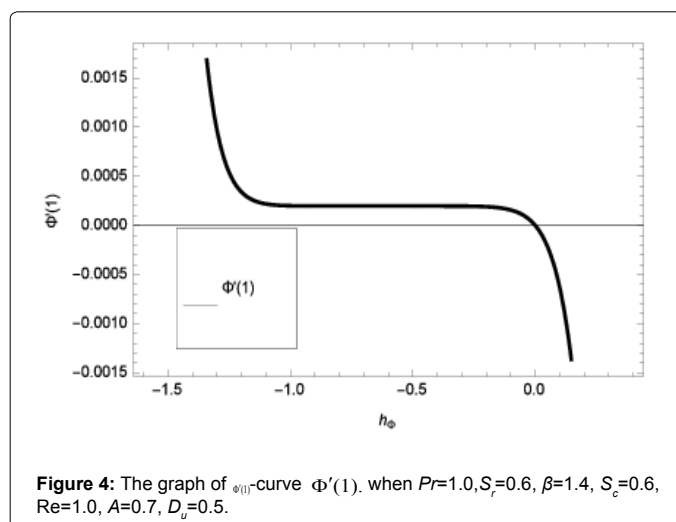
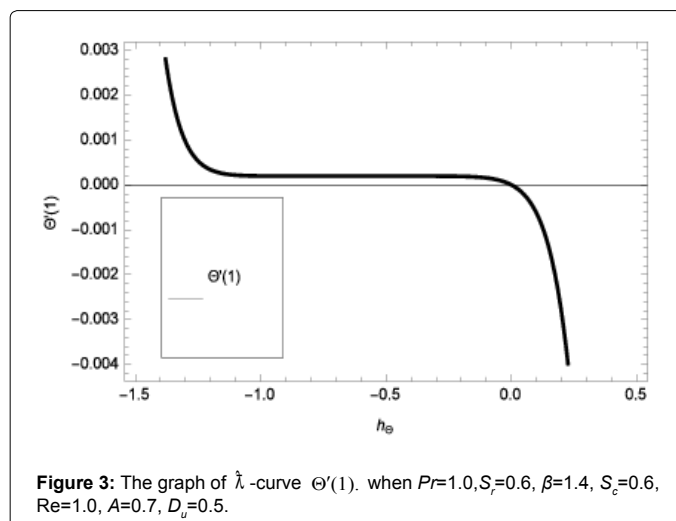
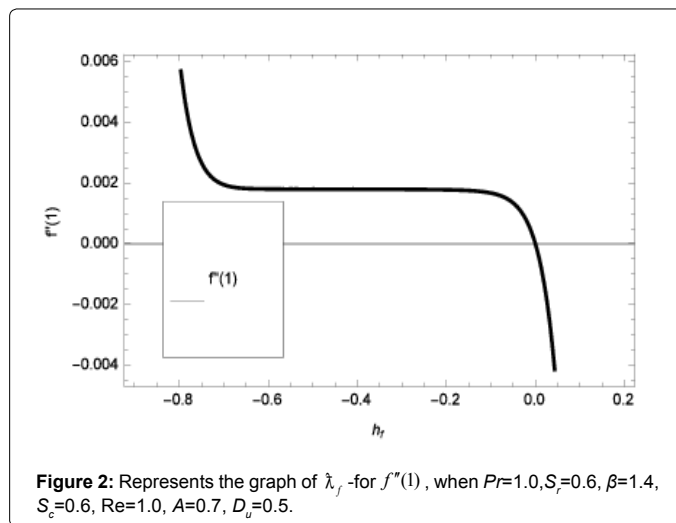
$$\lambda_\sigma = \begin{cases} 0, & \text{if } \rho \leq 1 \\ 1, & \text{if } \rho > 1 \end{cases}$$

HAM Solution Convergence

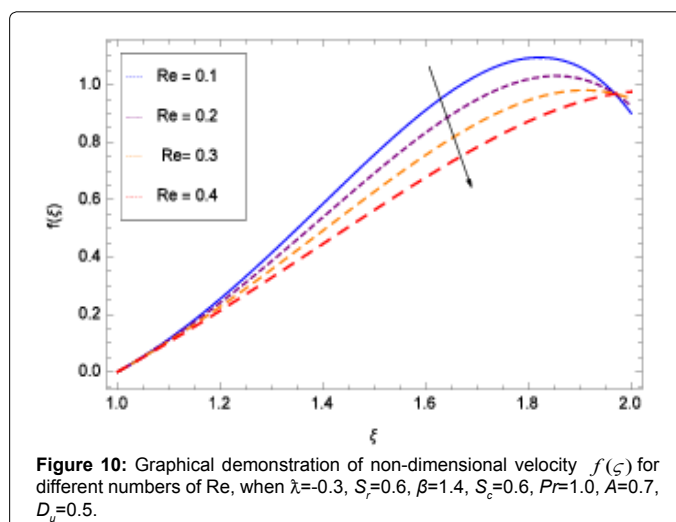
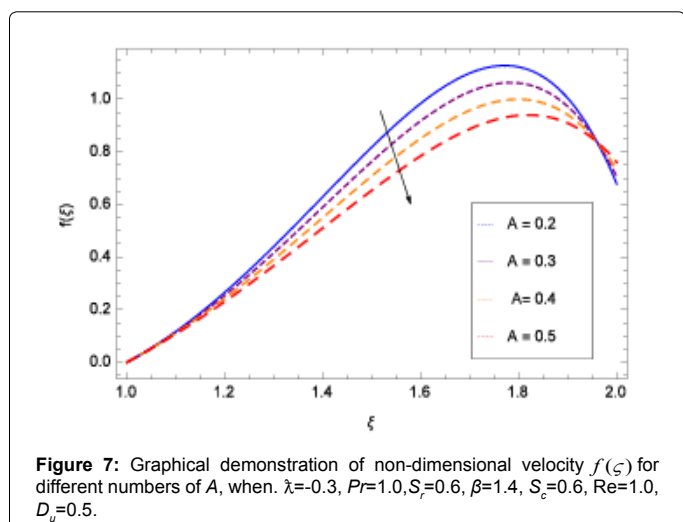
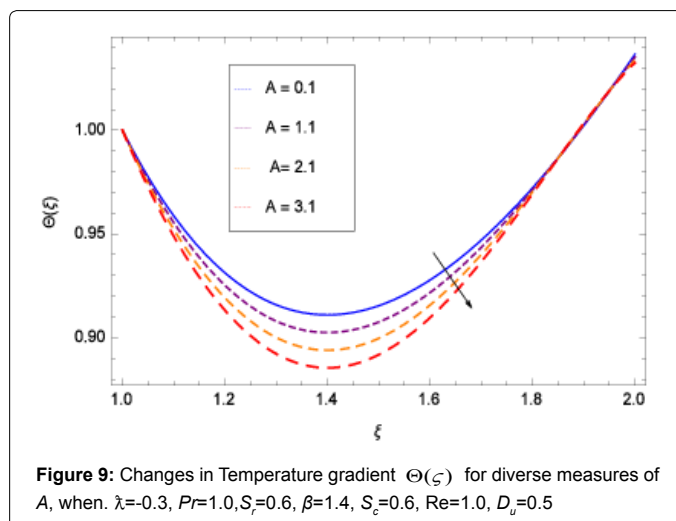
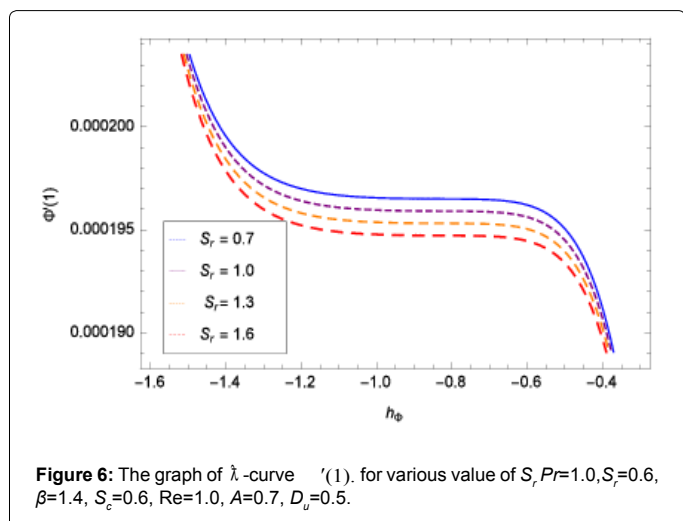
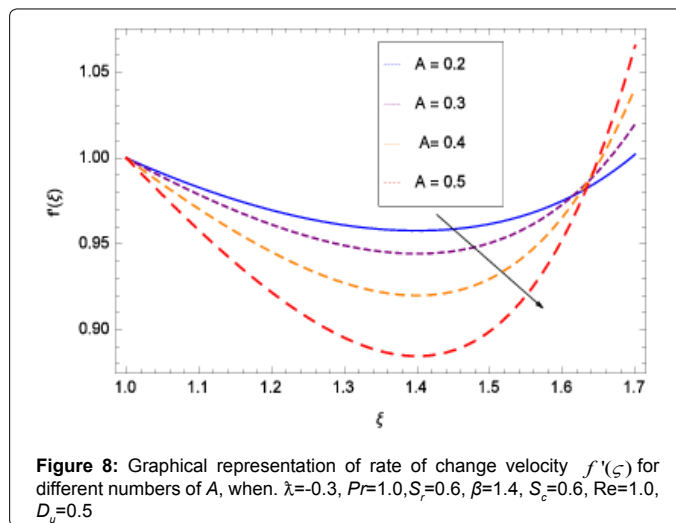
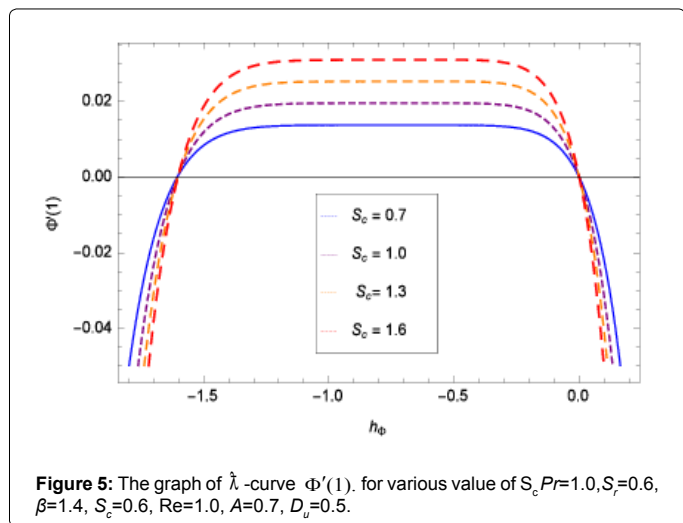
The convergence of eqn. (27), exclusively can be influenced by the auxiliary constraints λ_f , λ_Θ and λ_Φ . It is a selection in a manner which controls and converge the series answer Figure 1. The possibility segments of λ are plotted λ -curves of $f''(\eta)$, $\Theta'(\eta)$ and $\Phi'(\eta)$ for 20th order approximated HAM solution. The effective region of \hbar is $-0.7 < \lambda_f < -0.1, -1.2 < \lambda_\Theta < -0.1$ and $-1.2 < \lambda_\Phi < -0.1$. The convergence of the HAM method through λ -curves for velocity profile, temperature gradient and concentration field has been presented in Figures 2-4 respectively.

Results and Discussion

The performance of various physical constraints, enclosed in the flow field, like Reynolds quantities, Walter's B fluid parameter, Dufour number, Schmidt numbers, Soret number and Prandtl number on a non-dimensional velocity profile, temperature gradient and concentration field have been presented through graphs. The association of HAM approximation with Numerical method (ND-Solve Method) has been shown through graphs and tables. Figures 2-4 show the λ -curves of $f(\zeta), \Theta(\zeta), \Phi(\zeta)$ for the 20th-order probable HAM solution. Figure 5 and 6 shows that the convergent region for the problem shrinks when the value of Schmidt number and Soret number are increased. Figure 7 displays the velocity drop for the Walter's B fluid parameter A. The transport rate is decreased by increasing the value of A, and as a result the boundary-layer thickness is decreased. It is observed that thickness of the boundary-layer and velocity field



reduce by rising of Walter's B fluid parameter A. Whereas the elastic stress constraint rises with the thermal boundary layer thickness. While momentum boundary-layer thickness is decreased by increasing the values of A, consequence that the velocity field at the surface



of the cylinder increases. Figure 8 illustrates that Walter's B fluid constraint has the same effect on the velocity rate of change $f'(\xi)$. Figure 9 presents the effect of temperature gradient for several values of Walter's B fluid constraint A and it is detected that temperature

drops when Walter's B fluid parameter A is increased. The velocity distribution and rate of change of velocity field for several numbers of the Reynolds are specified in Figures 10 and 11. It is mentioned that the Reynolds quantity characterises the comparative consequence of the

inertia force against the viscous force and due to inertia the velocity is decreased. Actually the Reynolds quantity is the proportion of inertial and viscous forces. So in the Reynolds quantity the inertial force plays the central role as compared to viscous force. Therefore for by increasing larger Reynolds number the velocity decreases to zero and the flow degeneration is very slow. The same behaviour can be observed in Figures 12 and 13 for the temperature gradient and concentration profile i.e., temperature and concentration profile increase when Re increases. The reason for that bigger Reynolds number implies that inertial force exists as an overpowering agent in opposing the viscous force. Thin film constraint shows a special role in the fluid flow. From plot 14, it appears that the velocity profile reduces with larger values of film thickness parameter Figure 14. The more thick is the fluid film the more resistance offers in the flow and leads to retard the movement of the liquid. By increasing values of film thickness parameter the mass of fluid grows and as a result boundary layer thickness is decreased which causes retardation in the flow motion which is inversely related to the mass of the fluid. The thin film parameter plays a vital role in temperature distribution. Temperature reduces with larger magnitudes of thin film parameter which is observable in plot. 15. Heat is absorbed in the fluid film size, therefore, temperature of the fluid falls down as a result cooling effect is produced Figure 15. It is a fact that in non-Newtonian liquids the concentration is comparatively greater than that of the Newtonian liquids. The concentration is strongly dependent on film size parameter. The Concentration profile rises up with increasing values of thin film parameter as exhibited by Figure 16. The reason is that the film thickness has direct relation with viscosity and thermal conductivity which increase the concentration. The ratio of the momentum and thermal diffusivities represented the Prandtl quantity. In Figure 17 it is deliberated that the temperature gradient is a reducing function of Pr quantity. The temperature filed at the face of the cylinder attained some negative values for various numbers of Pr , i.e., heat is continuously transported from the surface of the cylinder to the fluid. Fluids that's having inferior Prandtl numbers holding upper thermal conductivities, so by this phenomenon heat are transferred from the sheet surface quicker with-in fluids with greater Prandtl quantity Pr . While in Figure 18 the concentration field displays a poor performance beside Prandtl values Pr because of the weakening of boundary layer. The consequence of the Dufour number of the heat and mass transference rate at the surface of the cylinder is demonstrated in Figures 19 and 20. Figure 19 shows the influence of Dufour quantity on the temperature field which reveals that Heat transfer is directly proportional to Dufour number. Actually, the Dufour Number is the proportion of the concentrations difference to temperature difference. When the Dufour Number D_u increases then concentration automatically increases consequently temperature falls down. Figure 20 is prepared for the effect of D_u number on Concentration. Since D_u defines the ratio of the concentrations difference to temperature difference. By increasing D_u , the viscosity improves and as a result the concentration increases and plotted that heat transmission rate reduces while the mass transmission rate rises with the increase of Dufour number. The same effects is observed for heat and mass transmission rates over Soret number. i.e., Figure 21 deliberates the effect of Soret number S_y over temperature gradient. It is seen that the heat transference rate increases with the rise of Soret number S_y . The cause is that Soret number shows the proportion of the temperatures difference to concentrations difference. This parameter exhibits that when S_y increases the temperature also increases. It means that the Soret number reductions the rate of heat transmission. Figure 22 displays the contribution of S_y in concentration. The Schmidt number is defined as the proportion of the viscid boundary films thickness and concentration boundary films thickness,

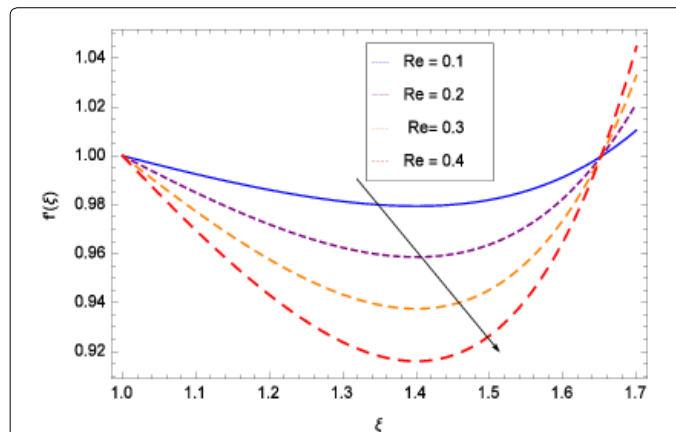


Figure 11: Graphical representation of rate of change of velocity $f'(\xi)$ for different numbers of Re, when $\lambda=-0.3, S_y=0.6, \beta=1.4, S_c=0.6, Pr=1.0, A=0.7, D_u=0.5$

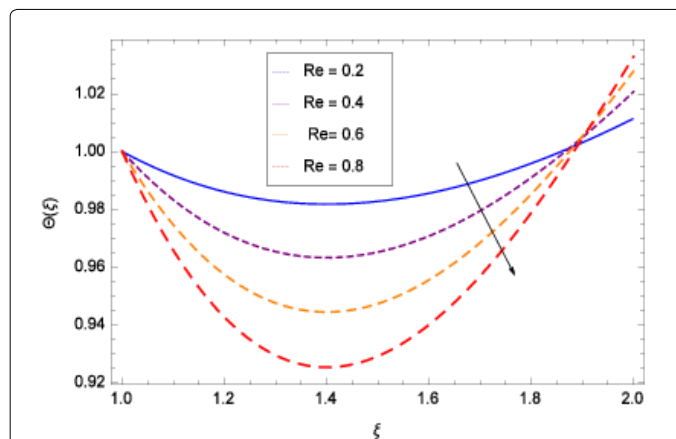


Figure 12: Changes in Temperature gradient $\Theta(\xi)$ for diverse measures of Re, when $\lambda=-0.3, Pr=1.0, S_y=0.6, \beta=1.4, S_c=0.6, A=0.7, D_u=0.5$.

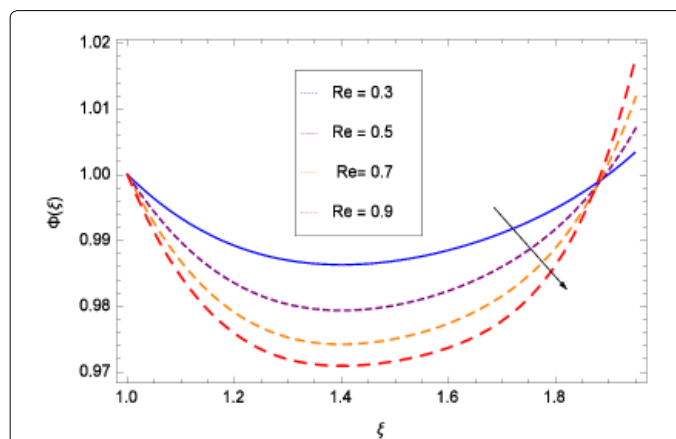
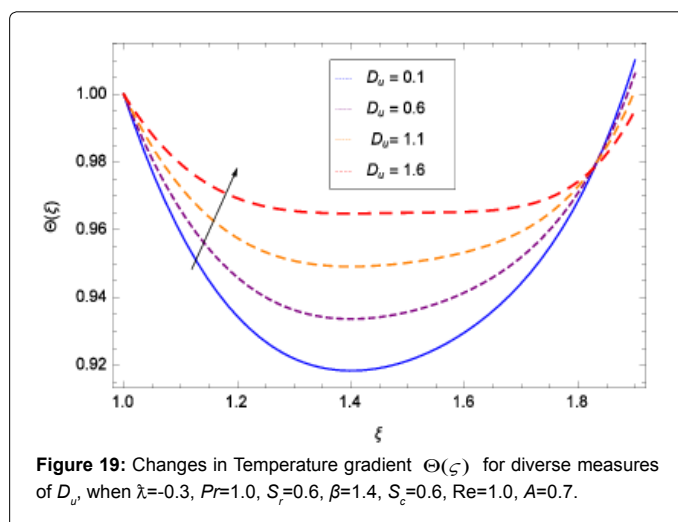
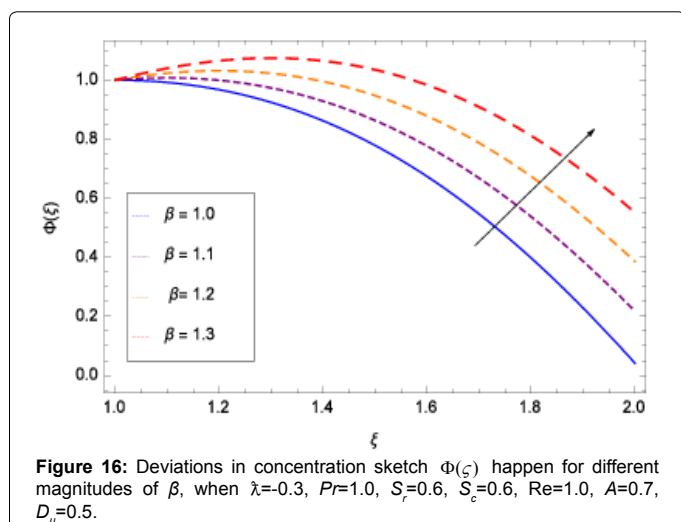
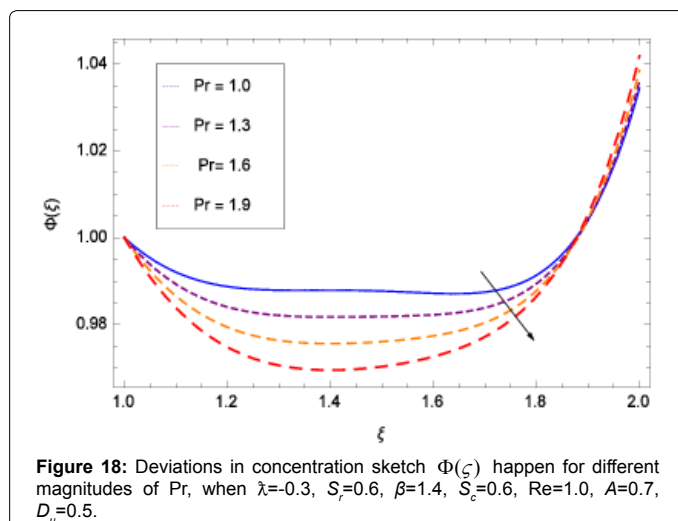
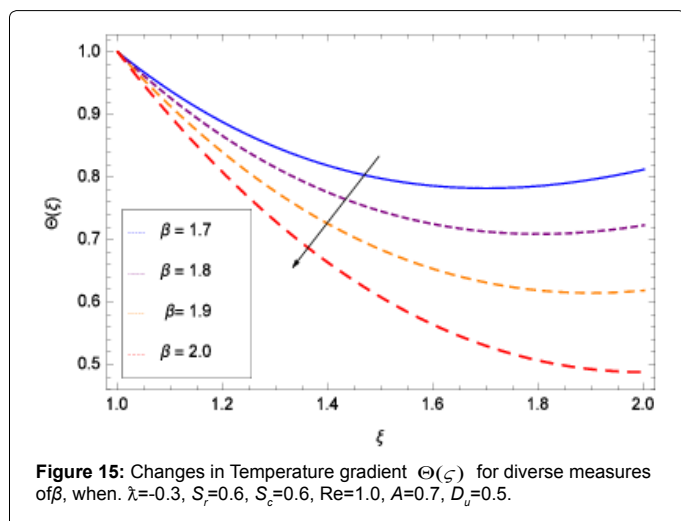
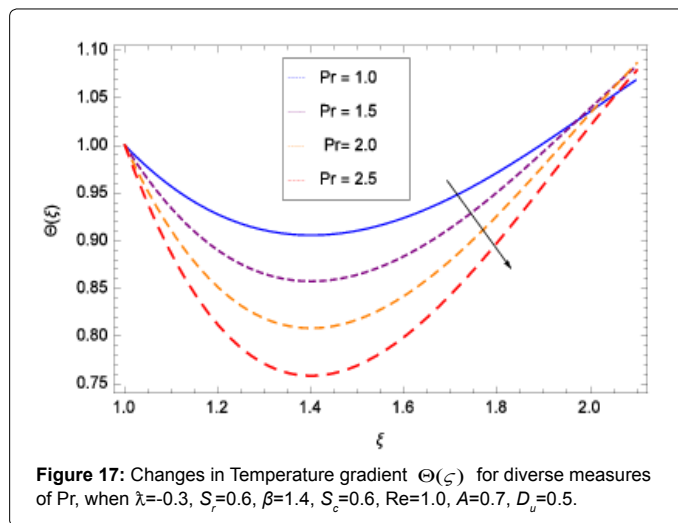
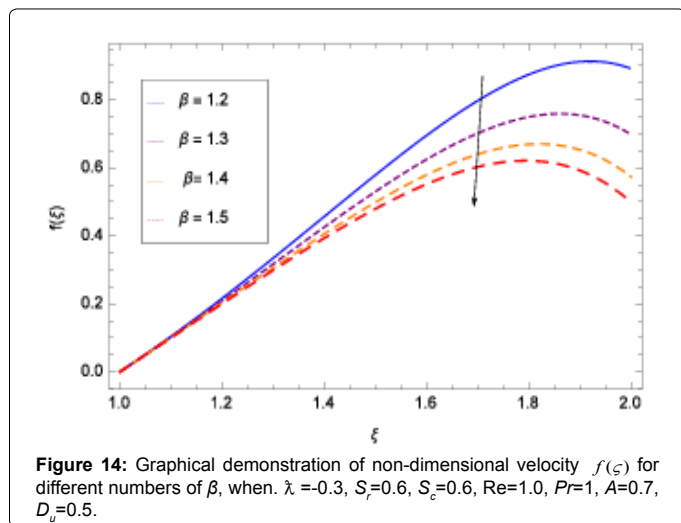


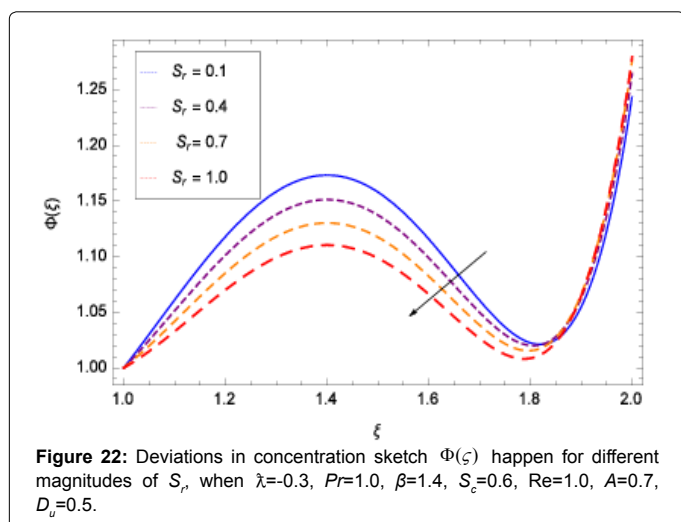
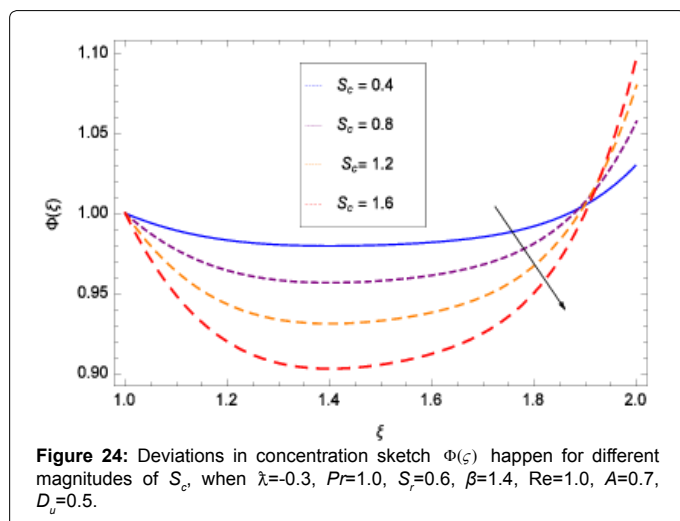
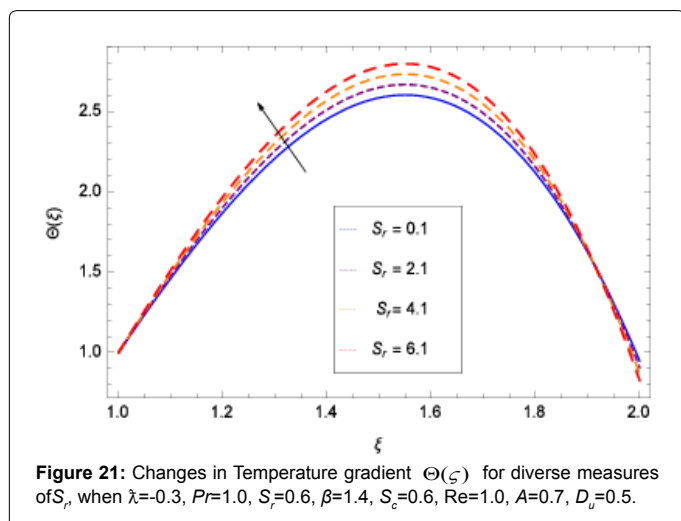
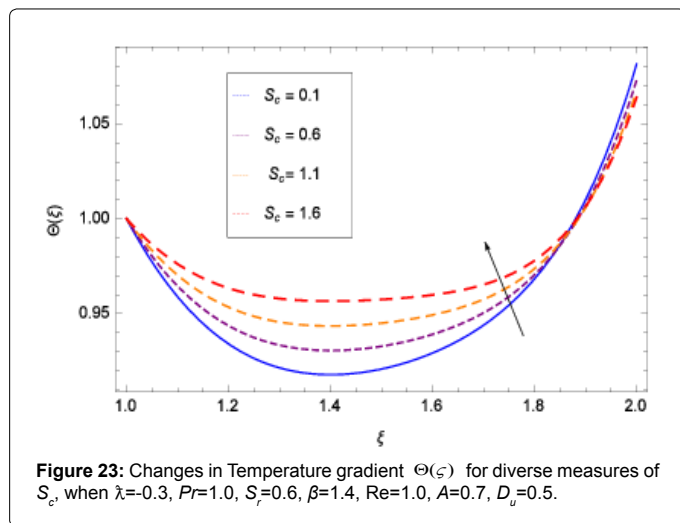
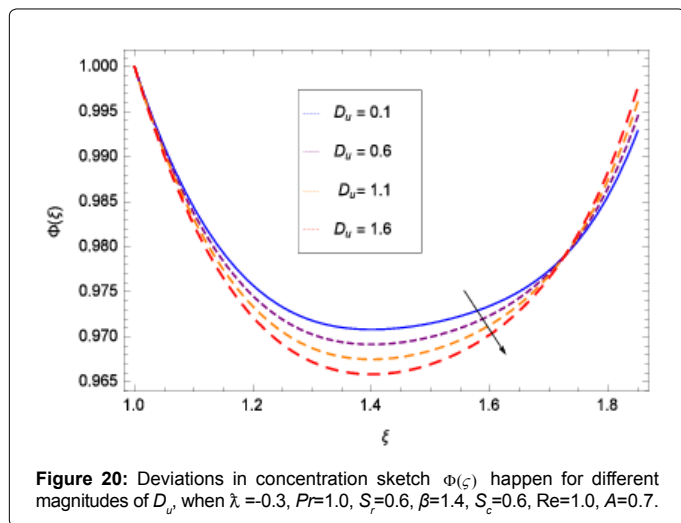
Figure 13: Deviations in concentration sketch $\Phi(\xi)$ happen for different magnitudes of Re, when $\lambda = -0.3, Pr=1.0, S_y=0.6, \beta=1.4, S_c=0.6, Re=1.0, A=0.7, D_u=0.5$.

which plays a vital role in heat and mass transmission procedures. When the Schmidt quantity is improved alternatively decreases the classes of concentration field and boundary-layer thickness and a small growth in the fluid temperature. Figure 23 represents the



effect of appropriate parameter S_c . The significance of the Schmidt number on the mass transmission rate is demonstrated in Figure 24. It is also shown that the mass transmission rate falls with the increase in Schmidt number. It is due to the reason that the concentration

boundary layer reductions with growth of Schmidt number S_c . The convergence of the solutions is shown in the Table 1 and it is observed from the table that momentum equation converges to 13th order of approximations whereas temperature distribution equation converges



Order of approximations	$-f''(1)$	$-\Theta'(1)$	$-\Phi'(1)$
1	0.000882667	0.00112000	0.00032000
5	0.00108098	0.00251398	0.000664943
10	0.00108378	0.00269044	0.000691743
15	0.00108382	0.00270355	0.000692040
20	0.00108382	0.00270458	0.000691927
25	0.00108382	0.00270467	0.000691907
30	0.00108382	0.00270468	0.000691905
32	0.00108382	0.00270468	0.000691904
33	0.00108382	0.00270468	0.000691904

Table 1: Displays the HAM approximated solutions convergent, when $\lambda = -0.4, Pr=0.7, S_r=0.2, \beta=1.1, S_c=0.2, Re=0.02, A=0.01, D_u=0.2$.

to 27th order of approximations and concentration equation converge up to 32nd order of approximations. Table 2 displays the performance of several implanted physical constraints on skin friction quantity. It is shown that skin friction quantity rises with the increase in fluid

film thickness parameter and Reynolds number while decreases the performance for Walter's B fluid constant. Table 3 is designed for the influence of various dynamic limitations on local Nusselt number. It is detected that the increase of Nusselt number is directly related to fluid film thickness parameter, Reynolds number and Prandtl number, while it is inversely related to Dufour number. Table 4 indicates the effect of included physical parameters on local Sherwood number and it is investigated that Sherwood number is increased for fluid film thickness parameter, Reynolds number and Schmidt number while decreases for

β	Re	A	$f''(1)$
1.1	0.02	0.01	0.00108382
1.12			0.00132709
1.14			0.00157984
1.1	0.02		0.00108382
	0.04		0.00216921
	0.06		0.00325616
	0.02	0.01	0.00108382
		0.02	0.008157
		0.04	0.00107921

Table 2: Demonstrates the Numerical results for skin friction factor for several physical constraints, when $\lambda=-0.4, Pr=0.7, S_r=0.2, =1.1, S_c=0.2, Re=0.02, A=0.01, D_v=0.2$.

β	Re	Pr	D_v	$-2k\theta'(1)$
1.1	0.02	0.7	0.2	0.00540936
1.12				0.00649177
1.14				0.00757428
1.1	0.02			0.00540936
	0.04			0.0108249
	0.06			0.0162466
	0.02	0.7		0.00540936
		0.8		0.00618764
		0.9		0.00696732
		0.7	0.2	0.00540936
			0.3	0.00531161
			0.4	0.00521331

Table 3: Demonstrates the Numerical values of local Nusselt number for various physical parameters, when $\lambda=-0.4, Pr=0.7, S_r=0.2, =1.1, S_c=0.2, Re=0.02, A=0.01, D_v=0.2$.

β	Re	S_c	S_r	$-\Phi'(1)$
1.1	0.02	0.2	0.2	0.000691905
1.12				0.000830282
1.14				0.000968655
1.1	0.02			0.000691905
	0.04			0.00138387
	0.06			0.00207589
	0.02	0.2		0.000691905
		0.3		0.00104088
		0.4		0.00139190
		0.2	0.2	0.000691905
			0.3	0.000637343
			0.4	0.000582473

Table 4: Demonstrates of the Sherwood quantity for various physical constraints, when $\lambda=-0.4, Pr=0.7, S_r=0.2, =1.1, S_c=0.2, Re=0.02, A=0.01, D_v=0.2$.

Soret number. The association of HAM and numerical methods for the velocity profile, temperature gradient and concentration field are displayed in Figures 25-27 and Tables 5-7 and shown that these two methods has adjacent solutions.

Conclusion

In the present work heat transmission distribution is examined analytically during thin film flow of a Walter's B fluid on a stretched cylinder. Applying an appropriate similarity transformations on the major equations of the flow problem and has been converted to non-linear ODEs. The obtained nonlinear equations are solved by HAM and numerical (ND solve) methods. The Consequence of the several

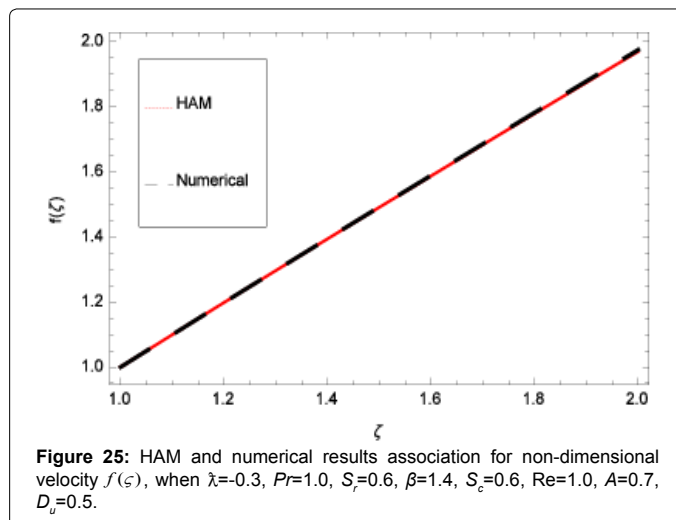


Figure 25: HAM and numerical results association for non-dimensional velocity $f(\zeta)$, when $\lambda=-0.3, Pr=1.0, S_r=0.6, \beta=1.4, S_c=0.6, Re=1.0, A=0.7, D_v=0.5$.

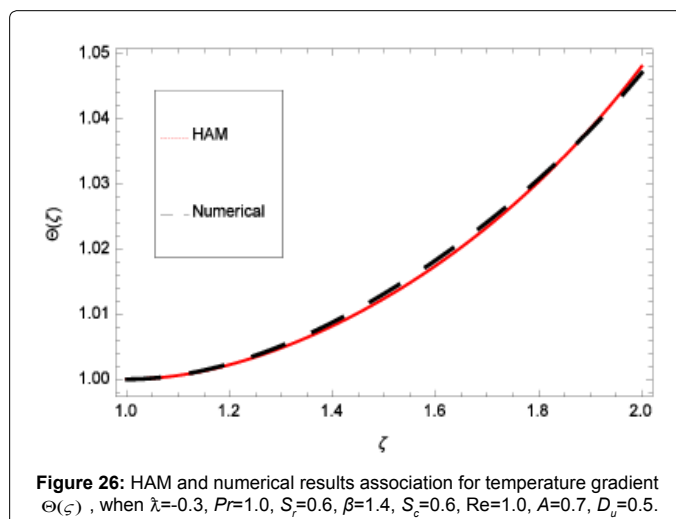


Figure 26: HAM and numerical results association for temperature gradient $\Theta(\zeta)$, when $\lambda=-0.3, Pr=1.0, S_r=0.6, \beta=1.4, S_c=0.6, Re=1.0, A=0.7, D_v=0.5$.

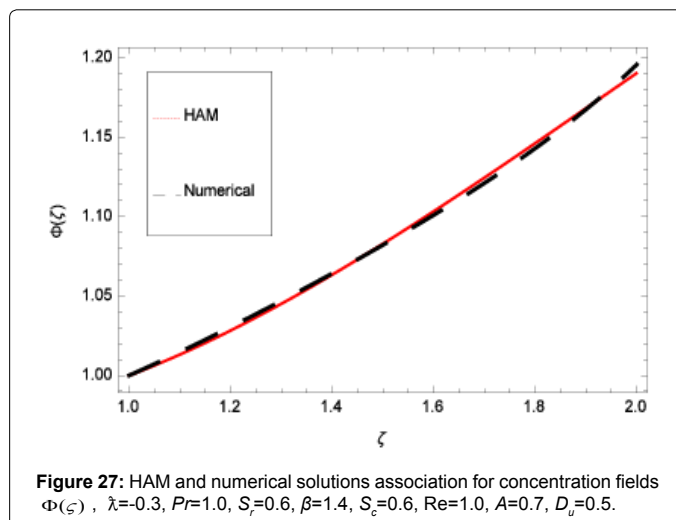


Figure 27: HAM and numerical solutions association for concentration fields $\Phi(\zeta)$, $\lambda=-0.3, Pr=1.0, S_r=0.6, \beta=1.4, S_c=0.6, Re=1.0, A=0.7, D_v=0.5$.

parameters are deliberated. The following assumptions can be observed from the analytical solution:

1. The velocity profile and rate of change of velocity profile both

ζ	HAM Result $f(\zeta)$	Numerical result	Absolute error
1.0	1.00000	1.00000	0.0
1.1	1.09959	1.09961	1.7×10^{-5}
1.2	1.19841	1.19851	9.7×10^{-5}
1.3	1.29651	1.29678	2.7×10^{-4}
1.4	1.39395	1.39452	5.7×10^{-4}
1.5	1.49081	1.49181	1.0×10^{-3}
1.6	1.58717	1.58874	1.6×10^{-3}
1.7	1.6831	1.68538	2.3×10^{-3}
1.8	1.7787	1.7818	3.1×10^{-3}
1.9	1.87407	1.87809	4.0×10^{-3}
2.0	1.96933	1.9743	5.0×10^{-3}

Table 5: The association between HAM and ND-Solve for non-dimensional velocity $f(\zeta)$ when $\lambda=-0.3, Pr=1.0, S_f=0.6, =1.4, S_c=0.6, Re=1.0, A=0.7, D_u=0.5$.

ζ	HAM Result $\Theta(\zeta)$	Numerical result	Absolute error
1.0	1.00000	1.00000	0.0
1.1	1.00059	1.00063	4.6×10^{-5}
1.2	1.00224	1.0024	1.6×10^{-4}
1.3	1.00481	1.00515	3.5×10^{-4}
1.4	1.00821	1.00876	5.5×10^{-4}
1.5	1.01242	1.01315	7.4×10^{-4}
1.6	1.01744	1.01827	8.3×10^{-4}
1.7	1.02337	1.02412	7.5×10^{-4}
1.8	1.03032	1.03075	4.2×10^{-4}
1.9	1.03847	1.03829	1.8×10^{-4}
2.0	1.04803	1.04704	9.9×10^{-4}

Table 6: The association between HAM and ND-Solve for temperature gradient $\Theta(\zeta)$ when $\lambda=-0.3, Pr=1.0, S_f=0.6, =1.4, S_c=0.6, Re=1.0, A=0.7, D_u=0.5$.

ζ	HAM Result $\Phi(\zeta)$	Numerical result	Absolute error
1.0	1.00000	1.00000	0.0
1.1	1.01313	1.01472	1.6×10^{-3}
1.2	1.02826	1.03045	2.2×10^{-3}
1.3	1.0451	1.04696	1.6×10^{-3}
1.4	1.06338	1.06416	7.8×10^{-4}
1.5	1.08285	1.0821	7.5×10^{-4}
1.6	1.10327	1.10094	2.3×10^{-3}
1.7	1.12444	1.12103	3.4×10^{-3}
1.8	1.14613	1.1429	3.2×10^{-3}
1.9	1.16814	1.16737	7.7×10^{-4}
2.0	1.19027	1.1956	5.3×10^{-3}

Table 7: The association between HAM and ND-Solve for concentration field $\Phi(\zeta)$ when $\lambda=-0.3, Pr=1.0, S_f=0.6, =1.4, S_c=0.6, Re=1.0, A=0.7, D_u=0.5$.

decreases by increasing the value of Walter's B fluid constant and Reynolds number.

- The same effect is concluded in temperature filed for Walter's B fluid constant and Reynolds number.
- The effect of Prandtl number is directly related to concentration field and inversely related to temperature filed.
- The temperature distribution increases by increasing Soret, Dufour and Schmidt numbers during fluid motion.
- While the concentration field is decreased by increasing the

values of Soret, Dufour and Schmidt numbers during fluid motion.

According to the prevailing literature this is the first effort concerning the heat distribution of a thin film flow of a Walter's B fluid on a stretching cylinder.

Competing Interests

All the writers state that they have no challenging securities.

Author's Contribution

TG and WK modelled the problem and solved. MI participated in the

physical discussion of the problem. All authors recited and acknowledged the last manuscript.

References

1. Wang CY (1990) Liquid film on an unsteady stretching surface. Q Appl Math 48: 601-610.
2. Usha R, Sridharan R (1995) The Axisymmetric Motion of a Liquid Film on an Unsteady Stretching Surface. J Fluids Eng 117: 81-85.
3. Liu IC, Andersson IH (2008) Heat transfer in a liquid film on an unsteady stretching sheet. Int J Thermal Sci 47: 766-772.
4. Aziz RC, Hashim I, Alomari AK (2011) Thin film flow and heat transfer on an unsteady stretching sheet with internal heating. Meccanica 46: 349-357.
5. Tawade J, Abel MS, Metri PG (2016) Thin film flow and heat transfer over an unsteady stretching sheet with thermal radiation, internal heating in presence of external magnetic field. Physics Flu 3: 29-40.
6. Andersson HI, Aarseth JB, Braud N, Dandapat BS (1996) Flow of a power-law fluid film on an unsteady stretching surface. J Non-Newtonian Fluid Mech 62: 1-8.
7. Chen CH (2003) Heat transfer in a power-law liquid film over an unsteady stretching sheet. Heat and Mass Transfer 39: 791-796.
8. Wang C, Pop I (2006) Analysis of the flow of a power-law liquid film on an unsteady stretching sheet by means of homotopy analysis method. J Non-Newtonian Fluid Mech 138: 161-172.
9. Chen CH (2006) Effect of viscous dissipation on heat transfer in a non-Newtonian liquid film over an unsteady stretching sheet. J Non-Newtonian Fluid Mech 135: 128-135.
10. Megahed AM (2015) Effect of slip velocity on Casson thin film flow and heat transfer due to unsteady stretching sheet in presence of variable heat flux and viscous dissipation. Appl Math Mech Engl 36: 1273-1284.
11. Abolbashari MH, Freidoonimehr N, Rashidi MM, Abolbashari MH, Nazari F, et al. (2015) Analytical modelling of entropy generation for Casson nano-fluid flow induced by a stretching surface. Adv Powder Technol 26: 542-552.
12. Qasim M, Khan ZH, Lopez RJ, Khan WA (2016) Heat and mass transfer in nanofluid thin film over an unsteady stretching sheet using Buongiorno's model. Eur Phys J Plus 131: 1-16.
13. Hussain A, Ullah A (2016) Boundary layer flow of a Walter's B fluid due to a stretching cylinder with temperature dependent viscosity. Alexandria Eng J 55: 3073-3080.
14. Manjunatha PT, Gireesha BJ, Prasannakumara BC (2014) Thermal analysis of conducting dusty fluid flow in a porous medium over a stretching cylinder in the presence of non-uniform source/sink. Int J Mech Mater Eng 9: 1-10.
15. Hayat T, Shafiq A, Alsaedi A (2015) MHD axisymmetric flow of third grade fluid by a stretching cylinder. Alexandria Eng J 54: 205-212.
16. Qasim M, Khan ZH, Khan WA, Shah IA (2014) MHD Boundary Layer Slip Flow and Heat Transfer of Ferrofluid along a Stretching Cylinder with Prescribed Heat Flux. PLoS ONE 9:1-6.
17. Sheikholeslami M (2014) Effect of uniform suction on nanofluid flow and heat transfer over a cylinder. J Braz Soc Mech Sci Eng 37: 1623-1633.
18. Manjunatha PT, Gireesha BJ, Prasannakumara BC (2017) Effect of Radiation on Flow and Heat Transfer of MHD Dusty Fluid Over a Stretching Cylinder Embedded in a Porous Medium in Presence of Heat Source. Int J Appl Comput Math 3: 293-310.
19. Abdulhameed M, Vieru D, Sharidan S (2016) Comparison of different pressure waveforms for heat transfer performance of oscillating flow in a circular cylinder. Eng Sci Technol Int J 19: 1040-1049.
20. Mahdy A (2015) Heat Transfer and Flow of a Casson fluid due to A Stretching Cylinder with the Soret and Dufour Effects. J Eng Phys Thermophys 88: 928-936.
21. Hakeem AKA, Ganesh NV, Ganga B (2014) Effect of heat radiation in a Walter's liquid B fluid over a stretching sheet with non-uniform heat source/sink and elastic deformation. J King Saud Univer- Eng Sci 26: 168-175.
22. Pandey SD, Nema KV, Sandep T (2016) Characteristic of Walter's B Visco-Elastic Nanofluid Layer Heated from Below. Int J Energy Eng 6: 7-13.
23. Liao SJ (1992) The proposed homotopy analysis method for the solution of nonlinear problems. Shangai Jiao Tong University, Shanghai.
24. Liao SJ (1999) An Explicit, totally Analytic Approximate Solution for Blasius Viscous Flow Problems. Int J Non-Linear Mech. 34: 759-778.
25. Liao SJ (2003) Beyond Perturbation: Introduction to the Homotopy Analysis Method. Chapman and Hall, CRC, Boca Raton, p: 336.
26. Liao SJ (2003) On the Analytic Solution of Magnetohydrodynamic Flows of Non-Newtonian Fluids over a Stretching Sheet. J Fluid Mech 488: 189-212.
27. Liao SJ (2004) On Homotopy Analysis Method for Nonlinear Problems. Appl Math Comput 147: 499-513.
28. Liao SJ (2006) An Analytic Solution of Unsteady Boundary Layer Flows Caused by Impulsively Stretching Plate. Commun Nonlinear Sci Numer Simu 11: 326-339.
29. Liao SJ (2012) Homotopy analysis method in nonlinear differential equations. Springer and Higher Education Press Heidelberg.
30. Liao SJ (2010) An optimal homotopy-analysis approach for strongly nonlinear differential equations. Comm Nonlinear Sc Num Simulation. 15: 2003-2016.
31. Abbasbandy S (2006) The application of homotopy analysis method to nonlinear equations arising in heat transfer. Phys Lett A 360: 109-113.
32. Abbasbandy S (2007) Homotopy analysis method for heat radiation equations. Int Commun Heat Mass Trans 34: 380-388.
33. Abbasbandy S (2007) The application of homotopy analysis method to solve a generalized Hirota-Satsuma coupled KdV equation. Physics Letters A 361: 478-483.
34. Abbasbandy S, Shirzadi A (2011) A new application of the homotopy analysis method: Solving the Sturm-Liouville problems. Communications in Nonlinear Science and Numerical Simulation 16: 112-126.
35. Sheikholeslami M (2014) Effect of uniform suction of nanofluid flow and heat transfer over a cylinder. Braz Soc Mech Sci Eng 37: 1623-1633.
36. Khan NS, Gul T, Islam S, Khan I, Alqahtani AM, et al. (2017) Magneto hydrodynamic Nano liquid Thin Film Sprayed on a Stretching Cylinder with Heat Transfer. Appl Sci 7: 1-25.